

LSAP: Rethinking Inversion Fidelity, Perception and Editability in GAN Latent Space

Pu Cao^{1,2} Lu Yang¹ Dongxu Liu¹ Zhiwei Liu³ Shan Li¹ Qing Song^{1*}

¹Beijing University of Posts and Telecommunications ²Metavatar

³Institute of Automation Chinese Academy of Sciences

{caopu, soeaver, ldx, ls1995, priv}@bupt.edu.cn zhiwei.liu@nlpr.ia.ac.cn

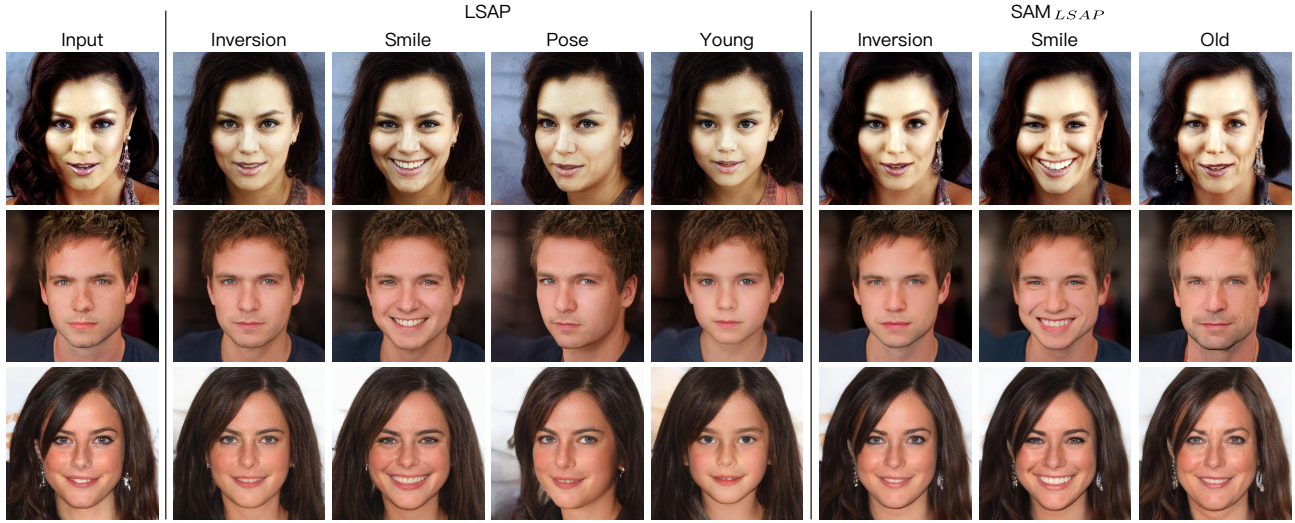


Figure 1: **Inversion and editing results from LSAP and SAM_{LSAP} [32].** Our method improves image quality and editability while retaining fidelity. It is compatible with the two-stage method and achieves better performance.

Abstract

As the research progresses, inversion is mainly divided into two steps. The first step is Image Embedding, in which an encoder or optimization process embeds images to get the corresponding latent codes. Afterward, the second step aims to refine the inversion and editing results, which we named Result Refinement. Although the second step significantly improves fidelity, perception and editability are almost unchanged and deeply depend on inverse latent codes from first step. Therefore, a crucial problem is gaining the latent codes with better perception and editability while retaining the reconstruction fidelity. In this work, we first point out that these two characteristics are related to the degree of alignment (or disalignment) of the inverse codes with the synthetic distribution. Then, we propose *Latent Space Alignment Inversion Paradigm (LSAP)*, which consists of an evaluation metric and solutions for inversion. Specifically, we introduce *Normalized Style Space*

(S^N space) and *Normalized Style Space Cosine Distance (NSCD)* to measure disalignment of inversion methods. Meanwhile, it can be optimized in both encoder-based and optimization-based embedding methods to conduct a uniform alignment solution. Extensive experiments in various domains demonstrate that NSCD effectively reflects perception and editability, and our alignment paradigm archives the state-of-the-art in both two stages. Code is available at <https://github.com/caopulan/GANInverter/tree/main/configs/lsap>.

1. Introduction

In recent years, Generative Adversarial Networks (GANs) [15] are used in various tasks [28, 51] and have dramatically improved image synthesis ability. Style-based generative models [23, 24, 22] further enhance the realism and resolution of image generation, achieving state-of-the-

art. The intermediate latent space \mathcal{W} space in StyleGAN encodes high-semantic information. As a strong prior, well-trained generator has demonstrated powerful capabilities and improved multiple tasks from traditional approaches, e.g., neural talking head [35, 53], face parsing [50, 57], and style transfer [29, 52].

These applications require latent codes, which are inherently available for synthetic images but cannot be applied directly to real images. To this end, inversion methods are designed to embed images into GAN’s latent space via various approaches. Existing works can be mainly divided into two stages. The first stage aims to attain latent codes, usually achieved by training an encoder or optimizing the reconstruction error, which we named *Image Embedding*. In the second stage, researchers employ diversiform strategies to improve inversion and editing results, e.g., predicting generator weights [4, 10], predicting intermediate feature [45, 32], and finetuning the generator [37, 11], which we named *Result Refinement*. Previous works [42] illustrate that fidelity, perception, and editability are three essential characteristics of inversion. However, in *Result Refinement*, more attention has been paid to improve fidelity, maintaining visual details like the background, hat, and eyeglasses while inheriting editability and perception by the inverse codes from first step. Hence, in order to achieve superior performance in these three characteristics simultaneously, a robust latent code embedding technique is still necessary.

The latent space from random sampling and transformation possesses a particular distribution, which we named synthetic distribution. Intuitively, latent codes from this distribution have better performance. Supervision from the discriminator constrains the sampled latent codes to generate photorealistic images. Moreover, editing directions are gained by sampling [38] and analyzing [18] in synthetic latent space. Hence, the key point of perception and editability is the alignment between inverse codes and synthetic distribution. An existing method [42] solves this problem by latent code discriminator and achieves more reasonable perception and editability. However, there are two significant shortcomings. Firstly, it limits the reconstruction performance since introducing a discriminator makes training unstable. Secondly, this approach cannot be applied to the optimization-based inversion methods. Therefore, our key motivation is the idea of constructing an alignment paradigm between embedding latent space and synthetic latent space which can be applied to both encoder-based and optimization-based inversion methods and retains reconstruction ability.

In this work, we thoroughly analyze the disalignment in inversion and propose the Latent Space Alignment Inversion Paradigm (LSAP). Specifically, we first introduce the Normalized Style Space (\mathcal{S}^N space). We prove that \mathcal{S}^N space is more suitable and efficient for measuring disalign-

ment than $\mathcal{Z}/\mathcal{W}/\mathcal{S}$ space. Moreover, we introduce a metric Normalized Style Space Cosine Distance (NSCD) to evaluate the inversion methods at latent code level, which have shown experimentally reflecting perception and editability. Then, we conduct the alignment solution in encoder-based and optimization-based methods, employing an alignment loss based on NSCD. We present extensive experiments to demonstrate the effects and generality of our alignment paradigm. We achieve the best trade-offs in encoder-based methods and drastically improve the perception and editability in the optimization-based method. Besides, we reach the state-of-the-art with HFGI [45], SAM [32], and PTI [37], which further demonstrates the potentiality and generality of our method. As shown in Figure 1, our visual results are natural and faithful. The key contributions of this work are summarized as follows:

- We rethink the fidelity, perception and editability in inversion task. As dividing inversion process into *Image Embedding* and *Result Refinement*, we point out that fidelity is enhanced in the second step while perception and editability are related to alignment between inverse codes and synthetic distribution.
- We propose an effective and generalized Latent Space Alignment Inversion Paradigm, including measurement and alignment solutions to improve perception and editability.
- To demonstrate the effect of our aligning paradigm, we take extensive experiments in various domains. NSCD reflects the perception and editability in a numerical way. Our alignment paradigm reaches better trade-offs between fidelity-perception and fidelity-editability. Applying to *Result Refinement* methods, LSAP_E achieves state-of-the-art.

2. Related Work

GAN Inversion. As we mentioned above, the inversion process can be divided into two steps. Firstly, an initial latent code is gained by optimization or encoder from a given image. Optimizing reconstruction error typically reach better fidelity, while it requires several minutes per image [24, 7, 1, 2]. Training an encoder [42, 36, 46, 16, 7] to invert images is efficient during inference but achieves inferior reconstruction results. The second step aims to refine the inversion and editing results, using various strategies. Some methods [4, 10] adjust the convolution weights of the generator by hypernetwork [17]. ReStyle [3] introduces an iterative refinement mechanism, refining the latent code by a residual-based encoder. HFGI [45] proposes a distortion consultation approach for high-fidelity reconstruction. SAM [32] inverses the different segments of image into different intermediate layer by predicting “invertibility”. Gen-

erator tuning [37, 11] can get the best inversion performance but is considerably time-consuming.

GAN-based Manipulation. Thanks to the rich semantic information of GAN’s [23, 24, 22] latent space, many works have proposed various methods to control generated results by manipulating latent representation. Some methods [9, 14, 40, 38] find editing directions of attributes (e.g., smile, gender, age, and pose) by semantic labels. Others find meaningful directions in an unsupervised [18, 39, 43, 44] or self-supervised [20, 34] way. Moreover, language-image models are explored to edit images by back-propagating the gradient of objective text [33]. Some works [41, 25] further introduce segmentation information to gain better performance, which may be extended to the human body by body GANs [12, 13] and human parsing techniques [49, 48, 50, 47] in the future. Since those manipulation approaches are almost built on latent codes, editability is also a crucial characteristic of inversion.

3. Latent Space Disalignment

In this section, we first rethink the source of fidelity, perception and editability, and we point out that the latter two are deeply related to the alignment (or disalignment) between inverse codes and synthetic distribution. To illustrate and address this problem in inversion task, we formulate the disalignment degree of inversion process.

3.1. Fidelity, Perception and editability

As first proposed by Tov *et al.* [42], fidelity¹, perception and editability are three vital characteristics of inversion methods. Fidelity measures the reconstruction ability, requiring methods embedding image into latent space which can reconstruct images faithfully. Perception evaluates the reconstructed images’ perceptual quality, consisting of sharpness and naturalness in practice. Besides, editability represents editing capability of inverse codes, which is a comprehensive measurement, including editing effects, attributes disentanglement, etc.

Source. We first trace these three characteristics. Minimizing image distortion is a significant objective function applied in all inversion methods. It gives the algorithm the ability to reconstruct given images faithfully. Perception is gained by the powerful generating capability of GANs, since generator is trained to generate the photorealistic results with high resolution by a discriminator. Editability benefits from the highly semantic latent space of GANs. Given the editing direction, we can modify the latent codes to edit corresponding attribute. However, the ability of perception and editability is conditional. Specifically, under the constraint from the discriminator, latent space in trained

¹Image distortion is originally used in e4e [42]. To represents the ability of inversion methods, we use *fidelity* instead of it.

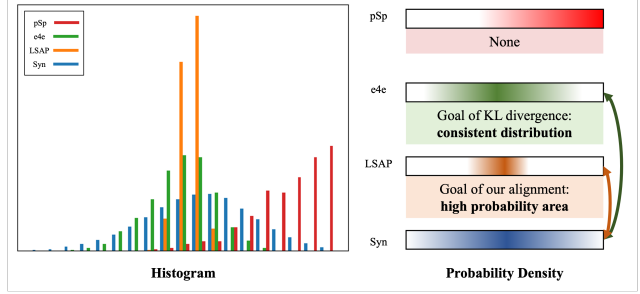


Figure 2: **Illustration of latent space distributions.** We invert all CelebA-HQ test split images to latent space and illustrate their distribution in \mathcal{S}^N space. Our alignment solution ensure that the embedded latent codes locate in high probability area of synthetic distribution, which protect the perception and editability.

GAN is required to fit dataset distribution, from which latent code can generate high-quality images. The generator may not generate good results from out-of-distribution latent code. That is also verified by latent code truncation, that codes near to mean code can generate high-quality results. Moreover, editing directions are obtained by sampling latent codes [38] or analyzing generator weights [39]. That is also built on a specific latent space in GAN. We name the latent space distribution in GAN as synthetic distribution, which is converted by pre-trained networks from multivariate normal standard distribution.

Impacts from two inversion stages. Inversion process can be divided into two stages: *Image Embedding* and *Result Refinement*. The latent codes are first attained by an encoder or optimized by minimizing image distortion. In this phase, reconstruction error is slightly large. In *Result Refinement* step, methods focus on recovering visual details (e.g., background, cloths) by adjusting weights [4] or intermediate features [45] of generator. This stage further improves the fidelity and even can invert the out-of-distribution images [37, 11]. However, perception and editability are inherited from the first step. In practice, if the inverse codes cannot be edited or generate images with good perceptual quality, the refined results still show the same effect. Hence, an essential problem is obtaining latent codes with better performance. In this work, **we focus on the first step to study fidelity, perception, and editability of latent codes.**

3.2. Disalignment Formulation

To illustrate disalignment between synthetic and inverse latent space, we firstly define \mathcal{P} space as a reference space, denoting \mathcal{P}_{inv} and \mathcal{P}_{syn} as inverse and synthetic latent space, respectively. $G_{\mathcal{P}}$ is defined as the generator from \mathcal{P} space to image space. Suppose that \mathcal{Z} is the multivariate standard normal distribution and \mathcal{X} is the real image distribution. We establish two mapping functions $F : \mathcal{Z} \rightarrow \mathcal{P}_{syn}$

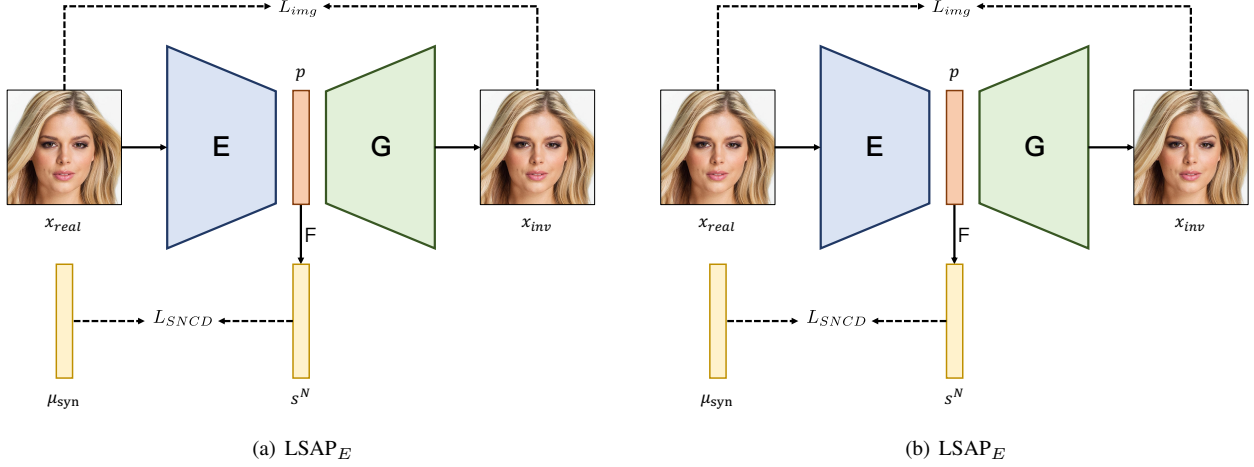


Figure 3: **Alignment inversion solutions of LSAP.** We show the details of encoder-based and optimization-based inversion methods in our alignment paradigm. The pivotal part is the L_{NSCD} , which represents the disalignment degree of inverse latent codes.

and $I : \mathcal{X} \rightarrow \mathcal{P}_{inv}$. In practice, I serves as an embedding method, used to convert images into \mathcal{P} space latent code. Moreover, F is a mapping function consisting of multiple parts in the front of generator. It is worth noting that aligning dose not mean making inverse distribution identical to synthetic distribution in this circumstance. It requires inverse codes located at high probability area in synthetic distribution. Hence we can define disalignment \mathcal{D} between these two spaces as follow:

$$\mathcal{D} = -\mathbb{E}_{x_{inv} \sim \mathcal{P}_{inv}} p_{syn}(x_{inv}) \quad (1)$$

Compared to Kullback-Leibler divergence. Another way to measure and optimize the disalignment is Kullback-Leibler divergence (KL divergence). In practice, latent code discriminator in e4e [42] can be considered as a method to minimize $D_{KL}(\mathcal{P}_{syn} || \mathcal{P}_{inv})$. However, as we analyzed above, aligning aims to let inverse codes have high probability in synthetic distribution, not to let these two distributions identical. Moreover, KL divergence can not be directly measured in inversion task. Hence it can not be used in optimization-based methods and served as a metric to indicate the characteristics of inversion methods. The difference also is also illustrated in Figure 2.

In Figure 1, two vital parts of disalignment measurement are which latent space is adequate to measure and how to measure $p_{syn}(x_{inv})$ for given sample. We will respectively answer these two questions in the following parts.

4. Latent Space Alignment Inversion Paradigm

In this section, we construct the **Latent Space Alignment Inversion Paradigm (LSAP)** to measure and improve perception and editability of inversion methods. Specifi-

cally, we introduce a new latent space Normalized Style Space (\mathcal{S}^N) and propose the Normalized Style Space Cosine Distance (NSCD) as a measurement. Moreover, we present generalized alignment solutions in *Image Embedding* phase, including LSAP_E and LSAP_O for encoder-based and optimization-based methods, respectively.

4.1. Normalized Style Space

Although $\mathcal{Z}/\mathcal{W}/\mathcal{W}^+$ spaces are primarily popular in previous research, in this work, we propose a new latent space, **Normalized Style Space (\mathcal{S}^N)**, and we will prove that it is better to measure disalignment.

Let us revisit the existing latent spaces first. Given the sampled random variable z from \mathcal{Z} space, the mapping network first converts it into w in \mathcal{W} space. Then affine modules are applied on w at each resolution level, which output is $s = \{s_1, s_2, \dots, s_k\}$, where $s_i = A_i w + b_i$ and the output space is named Style Space (\mathcal{S} space).

Property 4.1. Suppose that $s = \{s_1, s_2, \dots, s_k\}$ is a set of \mathcal{S} space latent codes and corresponding to image $x = G_{\mathcal{S}}(s)$. For $\forall a \in \mathbb{R}$ and $\forall l \in \{1, \dots, k\}$, if $s' = \{s'_1, s'_2, \dots, s'_k\}$ follows:

$$s'_i = \begin{cases} s_i, & i \neq l \\ a \times s_i, & i = l \end{cases}$$

we have $x = G_{\mathcal{S}}(s) = G_{\mathcal{S}}(s')$.²

Property 4.1 illustrates that \mathcal{S} space latent codes are scaled-independent in every component. Converting codes in the unit hyper-sphere, those codes with the same angles

²Proof can be found in Appendix.

will generate the same results. Based on this property, we construct a new latent space, Normalized Style Space (\mathcal{S}^N), in which codes are normalized from \mathcal{S} space by the euclidean norm. It follows:

$$s_i^N = \frac{s_i}{\|s_i\|_2} = \frac{A_i w + b_i}{\|A_i w + b_i\|_2} \quad (2)$$

To demonstrate differences between each latent space in measuring disalignment, we take extensive analyses:

Property 4.2. *Given a sets of \mathcal{S} space latent codes $s = \{s_1, \dots, s_k\} \neq \mathbf{0}$, $\exists s' = \{s'_1, \dots, s'_k\} \neq s$ such that $G_{\mathcal{S}}(s) = G_{\mathcal{S}}(s')$.*

Proof. According to Property 4.1, for $\forall l \in \{1, \dots, k\}$ when $s'_l = a \times s_l (a \in \mathbb{R})$ and $s'_i = s_i (i \neq l)$, we have $G_{\mathcal{S}}(s) = G_{\mathcal{S}}(s')$. Since $s_l \neq \mathbf{0}$, $s'_l \neq s_l$. \square

Property 4.3. *For l th layer ($\forall l \in \{1, \dots, k\}$), define $F_l : \mathcal{Z}/\mathcal{W} \rightarrow \mathcal{S}$ as the mapping function between \mathcal{S} and \mathcal{Z}/\mathcal{W} space. For all $p_l \in \mathcal{Z}/\mathcal{W}$ ($F_l(p) \neq \mathbf{0}$), exist $p'_l \neq p_l$ such that the corresponding \mathcal{S} space latent codes satisfy: $s'_l = a \times s_l (a \in \mathbb{R})$, where $s_l = F_l(p_l)$ and $s'_l = F_l(p'_l)$.³*

Corollary 4.1. *Given a sets of latent codes $p = \{p_1, \dots, p_k\}$ in $\mathcal{Z}/\mathcal{W}/\mathcal{S}$ space and $p \neq \mathbf{0}$, $\exists p' = \{p'_1, \dots, p'_k\} \neq p$ such that $G_{\mathcal{P}}(p) = G_{\mathcal{P}}(p')$.*

According to Corollary 4.1, different latent codes in $\mathcal{Z}/\mathcal{W}/\mathcal{S}$ space can generate the same images, which implies the disalignment degree of these latent codes can not reflect discrepancies in generated results. Hence, we choose \mathcal{S}^N as reference space to measure disalignment in inversion.

4.2. Normalized Style Space Cosine Distance

Illustrated in Figure 1, the probability of inverse latent codes in synthetic distribution is required to measure. However, it is difficult to calculate the $p_{syn}(x_{inv})$ straightforwardly, for the formula of p_{syn} is unknown. Motivated by latent code truncation, we find that using distance between inverse code and mean code instead of $p_{syn}(x_{inv})$ is a simple but efficient way. Code near mean code has a high probability practically. When we denote \mathcal{S}^N space as reference space, we can use cosine distance to measure disalignment and define NSCD as follow:

$$\begin{aligned} NSCD &= 1 - \mathbb{E}_{s_{inv} \sim \mathcal{S}_{inv}} [\cos(s_{inv}^N, \mu_{syn}^N)] \\ &= 1 - \mathbb{E}_{s_{inv} \sim \mathcal{S}_{inv}} [s_{inv}^N \cdot \mu_{syn}^T] \end{aligned} \quad (3)$$

Notably, as s_{inv}^N is the inversion result, cosine distance is differentiable for it to minimize in inversion process. The small value of NSCD means that \mathcal{S}_{inv}^N space aligns with \mathcal{S}_{syn}^N space. NSCD can reflect the perception and editability in image level, which we will show in qualitative and quantitative experiments.

³Proof can be found in Appendix.

4.3. Alignment Inversion

Inversion methods in *Image Embedding* phase aim to embed images into latent space in encoder-based or optimization-based way, and the process is as follows:

$$p^* = \arg \min_p [\mathcal{L}(x, G_{\mathcal{P}}(p))] \quad (4)$$

$$E^* = \arg \min_E [\mathbb{E}_{x \sim \mathcal{X}} (\mathcal{L}(x, G_{\mathcal{P}}(E(x))))] \quad (5)$$

where x is given image, \mathcal{X} is image dataset, \mathcal{L} is image level loss function (e.g., MSE, LPIPS [56], identity loss [8]) and E is an encoder. Since inversion methods are mainly supervised at the image level, there is a lack of limitation of inverse latent space distribution. To construct a uniform solution to train encoder or optimize the latent codes, we can constrain the disalignment degree by adding an alignment term in \mathcal{L} .

Thanks to NSCD's differentiable property, we can apply it to inversion methods to construct a direct and efficient alignment solution, shown in Figure 3. According to Equation 3, we first sample k ($k = 50,000$ in our experiments) latent codes from the multivariant normal distribution and convert them into \mathcal{S}^N by pre-trained generator to get mean code μ_{syn} . Then, we define an alignment loss as follows:

$$\mathcal{L}_{NSCD}(x) = 1 - (F(I(x)) \cdot \mu_{syn}^T) \quad (6)$$

where I is a *Image Embedding* method. \mathcal{L}_{NSCD} is calculated by given images x (i.e., a batch of images in encoder training or one image in optimization) in each iteration. Moreover, we present the details of our encoder and optimization methods separately.

Encoder. The pipeline of encoder-based alignment inversion method is shown in Figure 3(b). Given real images, encoder is optimized by minimizing multiple losses at image level and latent code level. Following [36] and [42], \mathcal{L}_{img} consists of distortion loss, perception loss, and identity loss. Besides, delta-regulation loss [42] is also applied to inverse codes, minimizing the deviation of \mathcal{W}^+ codes among each level. The whole training object is defined by:

$$\mathcal{L} = \mathcal{L}_2 + \lambda_1 \mathcal{L}_{lips} + \lambda_2 \mathcal{L}_{sim} + \lambda_3 \mathcal{L}_{d-reg} + \lambda \mathcal{L}_{NSCD} \quad (7)$$

where $\lambda_1, \lambda_2, \lambda_3, \lambda$ are hyper-parameters to adjust the weight of each component in loss function. In encoder-based method, \mathcal{L}_{NSCD} aims to align the encoder's output space with synthetic latent space.

Optimization. Optimization-based inversion method updates latent code iteratively. Compared to encoder-based approach, \mathcal{L}_{NSCD} is used to minimize the distance between a certain latent code with synthetic latent space. Following [24], we apply two losses in image level and latent code

level, respectively:

$$\mathcal{L} = \mathcal{L}_{lips} + \lambda \mathcal{L}_{NSCD} \quad (8)$$

The encoder-based and optimization-based method are denoted as LSAP_E and LSAP_O respectively.

5. Experiments

In this section, we conduct extensive experiments to demonstrate the effects of LSAP in various domains, including face, object (cars), scene (churches), and animal (wild animals). Implementation details can be found in Appendix.

Baselines. We take comprehensive comparisons in both two inversion stages. For *Image Embedding* methods, we compare our LSAP_E to pSp [36] and e4e [42] for encoder-based approaches and our LSAP_O to StyleGAN2 [24] projection for optimization-based approaches. Moreover, we evaluate e4e and LSAP_E's performance with four *Result Refinement* methods: ReStyle [3], HFGI [45], SAM [32] and PTI [37], where HFGI and SAM can be considered as intermediate feature prediction methods, and PTI is a generator tuning method.

Evaluation. We use MSE and LPIPS [56] to evaluate fidelity in all fields, and calculate identity similarity by ArcFace [8] between input and reconstructed images in face domain. To evaluate perception and editability, we use NSCD and latent editing consistency (LEC) [42]. Furthermore, we calculate the identity preservation between origin images and edited images under the same editing effects by each inversion method to demonstrate identity impacts during manipulation.

Method	Type	MSE ↓	Gain	LPIPS ↓	Similarity ↑
pSp [36]	<i>E</i>	0.0351		0.1628	0.5591
e4e [42]	<i>E</i>	0.0475		0.1991	0.4966
LSAP _E	<i>E</i>	0.0397		0.1766	0.5305
StyleGAN2- \mathcal{W} [24]	<i>O</i>	0.0696		0.1987	0.3066
LSAP _O - \mathcal{W}	<i>O</i>	0.0690		0.1986	0.2989
StyleGAN2- \mathcal{W}^+ [24]	<i>O</i>	0.0279		0.1179	0.7463
LSAP _O - \mathcal{W}^+	<i>O</i>	0.0359		0.1376	0.6587
ReStyle _{e4e} [3]	<i>E+L</i>	0.0429		0.1904	0.5062
ReStyle _{LSAP}	<i>E+L</i>	0.0296	-31.1%	0.1506	0.6148
HFGI _{e4e} [45]	<i>E+F</i>	0.0296		0.1172	0.6816
HFGI _{LSAP}	<i>E+F</i>	0.0210	-29.0%	0.0945	0.7405
SAM _{e4e} [32]	<i>E+F</i>	0.0143		0.1104	0.5568
SAM _{LSAP}	<i>E+F</i>	0.0117	-18.1%	0.0939	0.6184
PTI _{e4e} [37]	<i>E+T</i>	0.0074		0.0750	0.8633
PTI _{LSAP}	<i>E+T</i>	0.0067	-9.4%	0.0666	0.8696

Table 1: **Fidelity results on face domain.** We show the reconstruction results of encoder-based (*E*), optimization-based (*O*), and two-stage methods including latent codes refinement (*E+L*), feature prediction (*E+F*) and generator tuning (*E+T*), respectively. Gain refers to our improvement of MSE over the *X*+e4e baselines.

Method	NSCD	LEC / Similarity		
		Pose	Smile	Age
pSp	0.10	89.35/0.43	55.86/ 0.47	64.61/0.30
e4e	0.04	26.65/0.41	22.32/0.41	23.28/0.34
LSAP _E	0.03	19.02/0.45	14.03/0.45	14.67/0.39

Table 2: **Perception and editability results on face domain.** We compare NSCD, LEC [42], and identity similarity [8] between three encoder-based inversion methods.

Domain	Method	MSE ↓	LPIPS ↓	NSCD ↓
Car	e4e	0.1201	0.3252	0.0646
	LSAP _E	0.1049	0.3106	0.0492
Church	e4e	0.1505	0.4307	0.0761
	LSAP _E	0.1144	0.3426	0.0588
Wild Animal	e4e	0.0882 [†]	0.2658 [†]	0.0379 [†]
	LSAP _E	0.0785	0.2524	0.0224

Table 3: **Quantitative results on other domains.** [†] means the model is unavailable and we train the encoder by official code.

Quantitative Results. We provide the reconstruction results in Table 1 to evaluate fidelity on face domain. Our LSAP-based demonstrates outstanding performance in every baseline. Compared to pSp and StyleGAN2 projection, our additional alignment loss marginally sacrifices fidelity but improves perception and editability a lot which will be shown below. Meanwhile, LSAP_E attains superior performance than e4e. Applied to *Result Refinement* methods, LSAP_E outperforms e4e in all three methods. With ReStyle and HFGI, which use model to refine result and inference rapidly, LSAP_E gains about 30% improvement of MSE. PTI_{LSAP} gains best results in inversion.

In other domains, we compare LSAP_E to the most commonly used encoder e4e to illustrate the generality of our approach. Results are shown in Table 3. As can be seen, LSAP_E attains better performance in all three domains, which indicates our alignment solution is robust in GAN inversion task.

Moreover, we evaluate the perception and editability by NSCD, LEC and identity preservation during manipulation, which can be found in Table 2. LSAP_E achieves the best NSCD and LEC in three editing attributes and identity similarity in two attributes. It is worth mentioning that although e4e has decent editability, it gets worse identity preservation than pSp in "pose" and "smile", which is caused by their reconstruction gap. Nevertheless, LSAP_E reaches a higher similarity in "pose" and "age", which indicates that our approach can preserve portrait identity well during manipulation.

Qualitative Results. We perform the qualitative comparisons in Figure 4. For reconstruction ability of *Image Em-*



Figure 4: **Inversion and editing results of encoder-based and two-stage inversion methods on face domain.** We show the comparison of encoder-based, optimization-based and two-stage method respectively. LSAP_E improves the perception and editability while retaining the fidelity, and HFGI_{LSAP}, SAM_{LSAP} and PTI_{LSAP} further reduce image distortion.

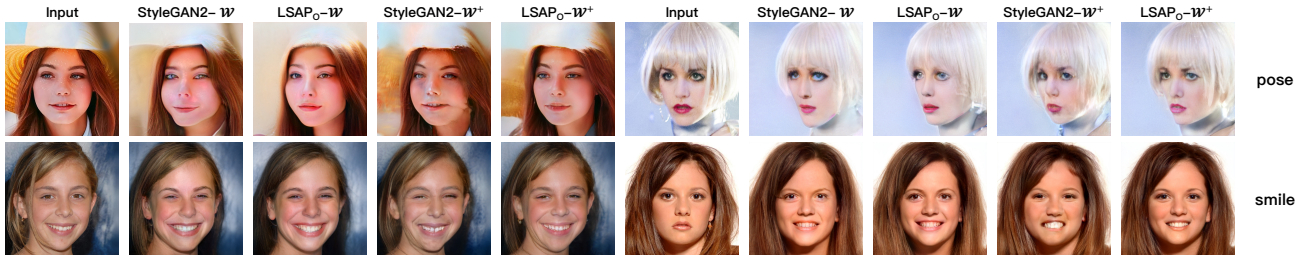


Figure 5: **Editability effects of LSAP for optimization-based methods.** LSAP makes optimized latent codes more editable and image quality is improved in both \mathcal{W} and \mathcal{W}^+ spaces.

bedding methods, our alignment paradigm attains comparable reconstruction quality with pSp. Meanwhile, LSAP improves image perception and editability a lot. In comparison with e4e, LSAP_E achieves better fidelity and editability. For example, editing results of the man in the first image of Figure 4 from e4e have redundant glasses (smile). In two-stage methods, HFGI, SAM and PTI improve the reconstruction capacity from e4e and LSAP_E. Inversion

results and editing effects from those methods are similar to the corresponding results from encoders while retaining more image details. PTI_{LSAP} achieves state-of-the-art for its high fidelity perception, and editability performance.

For optimization-based methods, our approach makes optimized code editable, which can be found in Figure 5. Vanilla projection in both \mathcal{W} and \mathcal{W}^+ spaces generate unnatural face details, while results significantly improve by

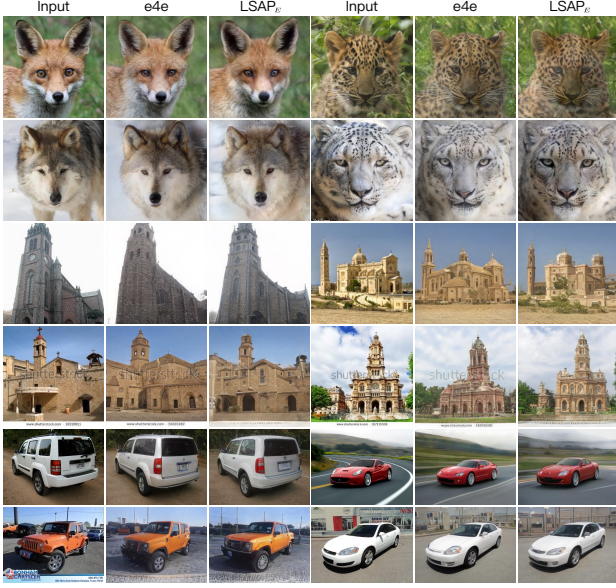


Figure 6: **Inversion results on other domains.** In car and church domains, the official e4e models are available and we train the encoder on AFHQ [6] Wild dataset.



Figure 7: **Inversion and editing comparison between e4e and LSAP_E.** We illustrate these two encoders’ inversion and editing results and the corresponding results with SAM. LSAP significantly improves editability and retains more visual details during inversion.

LSAP. It demonstrates that our approach provides a concise and straightforward solution even in optimization-based methods.

We further visualize inversion and editing results from e4e and LSAP_E in other domains, including cars, churches,

and wild animals. Result are demonstrated in Figure 6 and Figure 7. For inversion, LSAP_E achieves slight improvement in fidelity, since the color and reflection are reconstructed accurately. For example, in the second image of Figure 7, the reflection is represented in LSAP_E result, while the result from e4e only shows the white color. During editing, LSAP_E demonstrates the excellent ability to generate good editing results. With SAM technique, LSAP_E also achieves a better result in both inversion and manipulation.

Perception and Editability in Two Stages. In § 3.1, we point out that fidelity is improved in the *Result Refinement* step, while perception and editability are inherited from *Image Embedding*. As can be seen in Figure 4, when editing results from encoder are weak, such as attributes entanglement, the corresponding results from two-stage methods are basically similar. For example, editing the third image with “age”, results from e4e wear additional glasses, then the results from HFGI_{e4e}, SAM_{e4e}, and PTI_{e4e} also have the same impacts. Hence, although *Result Refinement* can largely improve the fidelity, the *Image Embedding* still plays an important role in inversion.

NSCD. In § 3 we find these two characteristics are related to alignment between inverse codes and synthetic distribution. Then we introduce that NSCD can numerically reflect them, which is validated in our experiments. Those with smaller NSCD have better image quality and editing results (e.g., e4e and LSAP_E), while the large NSCD means weak generating and manipulation results (e.g., pSp and StyleGAN2-W⁺). Compared to LEC [42], NSCD is evaluated on latent codes and irrelevant to editing vector, which is more general and convenient.

6. Conclusion

Fidelity, perception and editability are three critical characteristics of inversion methods. We start by tracing the source of fidelity, perception, and editability in inversion process and find that it is significant to embed images aligning with synthetic distribution in *Image Embedding* step, which also greatly impacts *Result Refinement* results. Hence, we propose a Latent Space Alignment Inversion Paradigm (LSAP), containing the measurement and solution of latent space disalignment. Specifically, to illustrate the disalignment straightforwardly and numerically, we propose Normalized Style Space Cosine Similarity (NSCD) as metric with Normalized Style Space (S^N) latent space. Thanks to the differentiable characteristic of NSCD, we conduct a uniform solution in encoder-based and optimization-based approaches. Through extensive experiments in four domains and three types baselines, LSAP shows promising results in all three features, and two-stage methods with LSAP achieve state-of-the-art.

References

- [1] Rameen Abdal, Yipeng Qin, and Peter Wonka. Image2stylegan: How to embed images into the stylegan latent space? In *Proceedings of the IEEE/CVF International Conference on Computer Vision*, pages 4432–4441, 2019. 2
- [2] Rameen Abdal, Yipeng Qin, and Peter Wonka. Image2stylegan++: How to edit the embedded images? In *Proceedings of the IEEE/CVF conference on computer vision and pattern recognition*, pages 8296–8305, 2020. 2
- [3] Yuval Alaluf, Or Patashnik, and Daniel Cohen-Or. Restyle: A residual-based stylegan encoder via iterative refinement. In *Proceedings of the IEEE/CVF International Conference on Computer Vision*, pages 6711–6720, 2021. 2, 6
- [4] Yuval Alaluf, Omer Tov, Ron Mokady, Rinon Gal, and Amit Bermanto. Hyperstyle: Stylegan inversion with hypernetworks for real image editing. In *Proceedings of the IEEE/CVF Conference on Computer Vision and Pattern Recognition*, pages 18511–18521, 2022. 2, 3
- [5] Xinlei Chen, Haoqi Fan, Ross Girshick, and Kaiming He. Improved baselines with momentum contrastive learning. *arXiv preprint arXiv:2003.04297*, 2020. 12
- [6] Yunje Choi, Youngjung Uh, Jaejun Yoo, and Jung-Woo Ha. Stargan v2: Diverse image synthesis for multiple domains. In *Proceedings of the IEEE/CVF conference on computer vision and pattern recognition*, pages 8188–8197, 2020. 8, 12
- [7] Antonia Creswell and Anil Anthony Bharath. Inverting the generator of a generative adversarial network. *IEEE transactions on neural networks and learning systems*, 30(7):1967–1974, 2018. 2
- [8] Jiankang Deng, Jia Guo, Niannan Xue, and Stefanos Zafeiriou. Arcface: Additive angular margin loss for deep face recognition. In *Proceedings of the IEEE/CVF conference on computer vision and pattern recognition*, pages 4690–4699, 2019. 5, 6, 12
- [9] Emily Denton, Ben Hutchinson, Margaret Mitchell, and Timnit Gebru. Detecting bias with generative counterfactual face attribute augmentation. 2019. 3
- [10] Tan M Dinh, Anh Tuan Tran, Rang Nguyen, and Binh-Son Hua. Hyperinverter: Improving stylegan inversion via hypernetwork. In *Proceedings of the IEEE/CVF Conference on Computer Vision and Pattern Recognition*, pages 11389–11398, 2022. 2
- [11] Qianli Feng, Viraj Shah, Raghudeep Gadde, Pietro Perona, and Aleix Martinez. Near perfect gan inversion. *arXiv preprint arXiv:2202.11833*, 2022. 2, 3
- [12] Anna Frühstück, Krishna Kumar Singh, Eli Shechtman, Niloy J Mitra, Peter Wonka, and Jingwan Lu. Insetgan for full-body image generation. In *Proceedings of the IEEE/CVF Conference on Computer Vision and Pattern Recognition*, pages 7723–7732, 2022. 3
- [13] Jianglin Fu, Shikai Li, Yuming Jiang, Kwan-Yee Lin, Chen Qian, Chen Change Loy, Wayne Wu, and Ziwei Liu. Stylegan-human: A data-centric odyssey of human generation. *arXiv preprint arXiv:2204.11823*, 2022. 3
- [14] Lore Goetschalckx, Alex Andonian, Aude Oliva, and Phillip Isola. Ganalyze: Toward visual definitions of cognitive image properties. In *Proceedings of the IEEE/CVF International Conference on Computer Vision*, pages 5744–5753, 2019. 3
- [15] Ian Goodfellow, Jean Pouget-Abadie, Mehdi Mirza, Bing Xu, David Warde-Farley, Sherjil Ozair, Aaron Courville, and Yoshua Bengio. Generative adversarial nets. *Advances in neural information processing systems*, 27, 2014. 1
- [16] Shanyan Guan, Ying Tai, Bingbing Ni, Feida Zhu, Feiyue Huang, and Xiaokang Yang. Collaborative learning for faster stylegan embedding. *arXiv preprint arXiv:2007.01758*, 2020. 2
- [17] David Ha, Andrew Dai, and Quoc V Le. Hypernetworks. *arXiv preprint arXiv:1609.09106*, 2016. 2
- [18] Erik Härkönen, Aaron Hertzmann, Jaakko Lehtinen, and Sylvain Paris. Ganspace: Discovering interpretable gan controls. *Advances in Neural Information Processing Systems*, 33:9841–9850, 2020. 2, 3, 12
- [19] Kaiming He, Xiangyu Zhang, Shaoqing Ren, and Jian Sun. Deep residual learning for image recognition. In *Proceedings of the IEEE conference on computer vision and pattern recognition*, pages 770–778, 2016. 12
- [20] Ali Jahanian, Lucy Chai, and Phillip Isola. On the “steerability” of generative adversarial networks. *arXiv preprint arXiv:1907.07171*, 2019. 3
- [21] Tero Karras, Timo Aila, Samuli Laine, and Jaakko Lehtinen. Progressive growing of gans for improved quality, stability, and variation. *arXiv preprint arXiv:1710.10196*, 2017. 12
- [22] Tero Karras, Miika Aittala, Samuli Laine, Erik Härkönen, Janne Hellsten, Jaakko Lehtinen, and Timo Aila. Alias-free generative adversarial networks. *Advances in Neural Information Processing Systems*, 34:852–863, 2021. 1, 3
- [23] Tero Karras, Samuli Laine, and Timo Aila. A style-based generator architecture for generative adversarial networks. In *Proceedings of the IEEE/CVF conference on computer vision and pattern recognition*, pages 4401–4410, 2019. 1, 3, 12
- [24] Tero Karras, Samuli Laine, Miika Aittala, Janne Hellsten, Jaakko Lehtinen, and Timo Aila. Analyzing and improving the image quality of stylegan. In *Proceedings of the IEEE/CVF conference on computer vision and pattern recognition*, pages 8110–8119, 2020. 1, 2, 3, 5, 6, 12
- [25] Taewoo Kim, Chaeyeon Chung, Yoonseo Kim, Sunghyun Park, Kangyeol Kim, and Jaegul Choo. Style your hair: Latent optimization for pose-invariant hairstyle transfer via local-style-aware hair alignment. *arXiv preprint arXiv:2208.07765*, 2022. 3
- [26] Diederik P Kingma and Jimmy Ba. Adam: A method for stochastic optimization. *arXiv preprint arXiv:1412.6980*, 2014. 12
- [27] Jonathan Krause, Michael Stark, Jia Deng, and Li Fei-Fei. 3d object representations for fine-grained categorization. In *Proceedings of the IEEE international conference on computer vision workshops*, pages 554–561, 2013. 12
- [28] Christian Ledig, Lucas Theis, Ferenc Huszár, Jose Caballero, Andrew Cunningham, Alejandro Acosta, Andrew Aitken, Alykhan Tejani, Johannes Totz, Zehan Wang, et al. Photo-realistic single image super-resolution using a generative adversarial network. In *Proceedings of the IEEE conference on*

- computer vision and pattern recognition*, pages 4681–4690, 2017. [1](#)
- [29] Zuoxin Li, Fuqiang Zhou, Lu Yang, Xiaojie Li, and Juan Li. Accelerate neural style transfer with super-resolution. *Multimedia Tools and Applications*, 79(7):4347–4364, 2020. [2](#)
- [30] Liyuan Liu, Haoming Jiang, Pengcheng He, Weizhu Chen, Xiaodong Liu, Jianfeng Gao, and Jiawei Han. On the variance of the adaptive learning rate and beyond. *arXiv preprint arXiv:1908.03265*, 2019. [12](#)
- [31] Ziwei Liu, Ping Luo, Xiaogang Wang, and Xiaoou Tang. Deep learning face attributes in the wild. In *Proceedings of the IEEE international conference on computer vision*, pages 3730–3738, 2015. [12](#)
- [32] Gaurav Parmar, Yijun Li, Jingwan Lu, Richard Zhang, Jun-Yan Zhu, and Krishna Kumar Singh. Spatially-adaptive multilayer selection for gan inversion and editing. In *Proceedings of the IEEE/CVF Conference on Computer Vision and Pattern Recognition*, pages 11399–11409, 2022. [1, 2, 6, 12](#)
- [33] Or Patashnik, Zongze Wu, Eli Shechtman, Daniel Cohen-Or, and Dani Lischinski. Styleclip: Text-driven manipulation of stylegan imagery. In *Proceedings of the IEEE/CVF International Conference on Computer Vision*, pages 2085–2094, 2021. [3](#)
- [34] Antoine Plumerault, Hervé Le Borgne, and Céline Hudelot. Controlling generative models with continuous factors of variations. *arXiv preprint arXiv:2001.10238*, 2020. [3](#)
- [35] KR Prajwal, Rudrabha Mukhopadhyay, Vinay P Namboodiri, and CV Jawahar. A lip sync expert is all you need for speech to lip generation in the wild. In *Proceedings of the 28th ACM International Conference on Multimedia*, pages 484–492, 2020. [2](#)
- [36] Elad Richardson, Yuval Alaluf, Or Patashnik, Yotam Nitzan, Yaniv Azar, Stav Shapiro, and Daniel Cohen-Or. Encoding in style: a stylegan encoder for image-to-image translation. In *Proceedings of the IEEE/CVF conference on computer vision and pattern recognition*, pages 2287–2296, 2021. [2, 5, 6, 12](#)
- [37] Daniel Roich, Ron Mokady, Amit H Bermano, and Daniel Cohen-Or. Pivotal tuning for latent-based editing of real images. *ACM Trans. Graph.*, 2021. [2, 3, 6, 12](#)
- [38] Yujun Shen, Ceyuan Yang, Xiaoou Tang, and Bolei Zhou. Interfacegan: Interpreting the disentangled face representation learned by gans. *IEEE transactions on pattern analysis and machine intelligence*, 2020. [2, 3, 12](#)
- [39] Yujun Shen and Bolei Zhou. Closed-form factorization of latent semantics in gans. In *Proceedings of the IEEE/CVF Conference on Computer Vision and Pattern Recognition*, pages 1532–1540, 2021. [3](#)
- [40] Nurit Spingarn-Eliezer, Ron Banner, and Tomer Michaeli. Gan” steerability” without optimization. *arXiv preprint arXiv:2012.05328*, 2020. [3](#)
- [41] Jiaze Sun, Binod Bhattarai, Zhixiang Chen, and Tae-Kyun Kim. Secgan: Parallel conditional generative adversarial networks for face editing via semantic consistency. *arXiv preprint arXiv:2111.09298*, 2021. [3](#)
- [42] Omer Tov, Yuval Alaluf, Yotam Nitzan, Or Patashnik, and Daniel Cohen-Or. Designing an encoder for stylegan image manipulation. *ACM Transactions on Graphics (TOG)*, 40(4):1–14, 2021. [2, 3, 4, 5, 6, 8, 12](#)
- [43] Andrey Voynov and Artem Babenko. Unsupervised discovery of interpretable directions in the gan latent space. In *International conference on machine learning*, pages 9786–9796. PMLR, 2020. [3](#)
- [44] Bin Xu Wang and Carlos R Ponce. The geometry of deep generative image models and its applications. *arXiv preprint arXiv:2101.06006*, 2021. [3](#)
- [45] Tengfei Wang, Yong Zhang, Yanbo Fan, Jue Wang, and Qifeng Chen. High-fidelity gan inversion for image attribute editing. In *Proceedings of the IEEE/CVF Conference on Computer Vision and Pattern Recognition*, pages 11379–11388, 2022. [2, 3, 6, 12](#)
- [46] Tianyi Wei, Dongdong Chen, Wenbo Zhou, Jing Liao, Weiming Zhang, Lu Yuan, Gang Hua, and Nenghai Yu. E2style: Improve the efficiency and effectiveness of stylegan inversion. *IEEE Transactions on Image Processing*, 31:3267–3280, 2022. [2](#)
- [47] Lu Yang, Zhiwei Liu, Tianfei Zhou, and Qing Song. Part decomposition and refinement network for human parsing. *IEEE/CAA Journal of Automatica Sinica*, 9(6):1111–1114, 2022. [3](#)
- [48] Lu Yang, Qing Song, Zhihui Wang, Mengjie Hu, Chun Liu, Xueshi Xin, Wenhe Jia, and Songcen Xu. Renovating parsing r-cnn for accurate multiple human parsing. In *European Conference on Computer Vision*, pages 421–437. Springer, 2020. [3](#)
- [49] Lu Yang, Qing Song, Zhihui Wang, and Ming Jiang. Parsing r-cnn for instance-level human analysis. In *Proceedings of the IEEE/CVF Conference on Computer Vision and Pattern Recognition*, pages 364–373, 2019. [3](#)
- [50] Lu Yang, Qing Song, Zhihui Wang, Zhiwei Liu, Songcen Xu, and Zhihao Li. Quality-aware network for human parsing. *arXiv preprint arXiv:2103.05997*, 2021. [2, 3](#)
- [51] Lu Yang, Qing Song, and Yingqi Wu. Attacks on state-of-the-art face recognition using attentional adversarial attack generative network. *Multimedia tools and applications*, 80(1):855–875, 2021. [1](#)
- [52] Shuai Yang, Liming Jiang, Ziwei Liu, and Chen Change Loy. Pastiche master: Exemplar-based high-resolution portrait style transfer. In *Proceedings of the IEEE/CVF Conference on Computer Vision and Pattern Recognition*, pages 7693–7702, 2022. [2](#)
- [53] Fei Yin, Yong Zhang, Xiaodong Cun, Mingdeng Cao, Yanbo Fan, Xuan Wang, Qingyan Bai, Baoyuan Wu, Jue Wang, and Yujiu Yang. Styleheat: One-shot high-resolution editable talking face generation via pretrained stylegan. *arXiv preprint arXiv:2203.04036*, 2022. [2](#)
- [54] Fisher Yu, Ari Seff, Yinda Zhang, Shuran Song, Thomas Funkhouser, and Jianxiong Xiao. Lsun: Construction of a large-scale image dataset using deep learning with humans in the loop. *arXiv preprint arXiv:1506.03365*, 2015. [12](#)
- [55] Michael Zhang, James Lucas, Jimmy Ba, and Geoffrey E Hinton. Lookahead optimizer: k steps forward, 1 step

back. *Advances in neural information processing systems*, 32, 2019. 12

- [56] Richard Zhang, Phillip Isola, Alexei A Efros, Eli Shechtman, and Oliver Wang. The unreasonable effectiveness of deep features as a perceptual metric. In *Proceedings of the IEEE conference on computer vision and pattern recognition*, pages 586–595, 2018. 5, 6
- [57] Yuxuan Zhang, Huan Ling, Jun Gao, Kangxue Yin, Jean-Francois Lafleche, Adela Barriuso, Antonio Torralba, and Sanja Fidler. Datasetgan: Efficient labeled data factory with minimal human effort. In *Proceedings of the IEEE/CVF Conference on Computer Vision and Pattern Recognition*, pages 10145–10155, 2021. 2

A. Property Proof

In this section, we provide detailed proof of Property 4.1 and Property 4.3.

A.1. Proof of Property 4.1

Property 4.1 Suppose that $s = \{s_1, s_2, \dots, s_k\}$ is a set of style space latent codes and corresponds to image $x = G_S(s)$. For $\forall a \in \mathbb{R}$ and $\forall l \in \{1, \dots, k\}$, \hat{s} follows:

$$\hat{s}_n = \begin{cases} s_n, & \text{if } n \neq l \\ a \times s_n, & \text{if } n = l \end{cases}$$

We have $x = G_S(s) = G_S(\hat{s})$.

Proof. According to StyleGAN2, style latent codes are used in weight demodulation way. For l th layer, convolution layer weights $W_{i,j,k}$ are scaled by l th style latent codes s_l firstly:

$$W'_{ijk} = s_l^i \times W_{ijk}, \quad (9)$$

where i, j, k enumerate input feature maps, output feature maps and spatial footprint, respectively.

To integrate instance normalization in convolution layer, StyleGAN2 demodulates each output feature map by $\sigma_j = \sqrt{\sum_{i,k} W'_{ijk}{}^2}$, assuming that input activations are i.i.d. random variables with unit standard deviation (ignore ϵ used for numerical stable):

$$W''_{ijk} = \frac{W'_{ijk}}{\sqrt{\sum_{i,k} W'_{ijk}{}^2}} \quad (10)$$

Substitute formula 9 into formula 10, then we can reach:

$$W''_{ijk} = \frac{s_l^i \times W_{ijk}}{\sqrt{\sum_{i,k} (s_l^i \times W_{ijk})^2}} \quad (11)$$

Suppose that $\hat{s}_l = a \times s_l$,

$$\begin{aligned} \hat{W}''_{ijk} &= \frac{\hat{s}_l^i \times W_{ijk}}{\sqrt{\sum_{i,k} (\hat{s}_l^i \times W_{ijk})^2}} \\ &= \frac{a \times s_l^i \times W_{ijk}}{\sqrt{\sum_{i,k} (a \times s_l^i \times W_{ijk})^2}} \\ &= \frac{s_l^i \times W_{ijk}}{\sqrt{\sum_{i,k} (s_l^i \times W_{ijk})^2}} = W''_{ijk} \end{aligned} \quad (12)$$

Thus, if scale s by $a \in \mathbb{R}$ in an arbitrary layer, convolution weights are identical, meaning generated images are the same. \square

A.2. Proof of Property 4.3

Property 4.3 For l th layer ($\forall l \in \{1, \dots, k\}$), define $F_l : \mathcal{Z}/\mathcal{W} \rightarrow \mathcal{S}$ as the mapping function between \mathcal{S} and \mathcal{Z}/\mathcal{W} space. For $\forall p_l \in \mathcal{Z}/\mathcal{W}$ ($F_l(p) \neq \mathbf{0}$) and $a \in \mathbb{R}$, $\exists p'_l \neq p_l$ such that the corresponding \mathcal{S} space latent codes satisfy: $s'_l = a \times s_l$, where $s_l = F_l(p_l)$ and $s'_l = F_l(p'_l)$.

Proof. We prove this property separately under \mathcal{W} and \mathcal{Z} spaces. Since cases under each layer level are the same without loss of generality, to express concisely, we consider the situation under an arbitrary layer and ignore l in the later formulation.

\mathcal{W} space The mapping function between \mathcal{W} and \mathcal{S} space is established by linear projection in generator, as follows:

$$s = F(w) = Aw + b \quad (13)$$

If $\exists y$, such that

$$Ay = (a - 1)b \quad (14)$$

and let

$$w' = aw + y \quad (15)$$

we have

$$s' = Aw' + b = A(aw + y) + b = aAw + ab = as \quad (16)$$

In StyleGAN, $A \in \mathbb{R}^{m \times n}$ ($m \leq n$) may not be a square matrix in some resolution levels and the rank of A is unstable. It indicates Equation 14 can not be solved by inverse of A directly. We can obtain y by solving the least squares problem:

$$\min_y \|Ay - (a - 1)b\| \quad (17)$$

Hence, for $\forall w$, when $w' = aw + y$, $F(w) = a \cdot F(w')$. In addition, we can prove $w' \neq w$ by the counterfactual method. If $w' = w$, we have $y = (1 - a)w$ and $A(1 - a)w = (a - 1)b$, so $Aw = -b$ and $s = \mathbf{0}$. Due to $s \neq \mathbf{0}$, $w' \neq w$ and $w' = aw + y$, $F(w) = a \cdot F(w')$, we prove that property holds in \mathcal{W} space.

\mathcal{Z} space Although we have proved in \mathcal{W} space, the mapping function between \mathcal{Z} and \mathcal{W} or \mathcal{Z} and \mathcal{S} is represented by a multilayer perception, which is difficult to prove directly by formula. Fortunately, as the objective function is defined, we can obtain z' by optimization, satisfying $s = F(z) = a \times F(z') = ks'$ and $z' \neq z$. \square

B. Implementation Details

Datasets. We conduct the whole experiment on four domains: faces, cars, churches, and wild animals, corresponding to human, object, scene, and animal, respectively. In

all domains, we use the official StyleGAN2 generator. For face domain, We train the LSAP_E on FFHQ [23] (70,000 images) and evaluate on CelebA-HQ [31, 21] test dataset (2824 images). Editing directions are gained by [38]. For car domain, we use Stanford Cars [27] dataset with 8,144 images for training and randomly selected 1000 images for evaluation and edit images by [18]. For church domain, we use LSUN [54] Church dataset with 126,227 training images and 300 test images. For wild animal domain, we use AFHQ [6] Wild dataset.

LSAP_E. The input image resolution is 192×256 in car domain and 256×256 for the others. For data augmentation, we only employ random horizontal flips. We adopt the Ranger optimizer, combining the Rectified Adam [30] and the Lookahead technique [55], with 0.001 learning rate. We take all experiments on a single GPU with batch size of 8. Besides, we follow the progressive training from e4e [42]. In LSAP_E, perceptual loss λ_1 is 0.8, delta-regulation loss λ_3 is $2e - 5$, and NSCD loss λ is 0.5 for all domains. Similarity loss weight λ_2 is 0.1 for face domain over pre-trained ArcFace [8] and 0.5 for others with MOCOv2 [5] and ResNet-50 [19].

Optimization-based Method. Following [24], we adopt Adam [26] optimizer to minimize perceptual loss and NSCD loss with noise regularization. λ is set to 20 for \mathcal{W}^+ space and 5 for \mathcal{W} space.

Result Refinement Method. We apply e4e and LSAP_E to three *Result Refinement* methods, HFGI [45], SAM [32], and PTI [37] to illustrate the effects of *Image Embedding* step. For HFGI, we use official weight to evaluate HFGI_{e4e} and follow its training script to train HFGI_{LSAP}. In practice, we only replace the encoder weight from e4e to LSAP_E with the same architecture. Since SAM only releases the optimization codes, we first embed images into latent codes by encoders, and then optimize the latent codes with intermediate feature for 500 iterations, with threshold $\tau = 0.225$. For PTI, we use inverse codes by encoders as pivotal latent codes and tune the generator for 350 steps.

Evaluation Pipeline. Since inversion and editing results are gained by multiple codebases, we conduct all image level evaluations on saved image files. MSE, LPIPS and identity similarity are calculated on 256×256 resolution by script from pSp⁴ [36]. TFor LEC and identity similarity, we use different editing factor to ensure the same editing effect for all inversion methods, which can be found in qualitative results.

C. Ablation Study

We study the hyper-parameter λ of \mathcal{L}_{NSCD} on face domain with LSAP_E as example, and the quantitative results

⁴<https://github.com/eladrich/pixel2style2pixel>

λ	Fidelity			Perception & editability			
	MSE ↓	LPIPS ↓	Similarity ↑	NSCD ↓	LEC _{pose} ↓	LEC _{smile} ↓	LEC _{age} ↓
0	0.0369	0.1657	0.5512	0.0736	24.8245	22.5007	24.8069
0.1	0.0382	0.1703	0.5438	0.0416	19.1594	14.0133	15.2246
0.25	0.0391	0.1737	0.5410	0.0395	19.1345	14.1382	15.1599
0.5	0.0397	0.1766	0.5305	0.0385	19.0211	14.0360	14.6715
0.75	0.0406	0.1792	0.5222	0.0381	19.0949	14.0128	14.3198
1.0	0.0413	0.1809	0.5168	0.0378	15.8013	13.8433	14.6084

Table 4: **Ablation study on hyper-parameter of LSAP_E.** We set $\lambda = 0.5$ in our experiments by default.

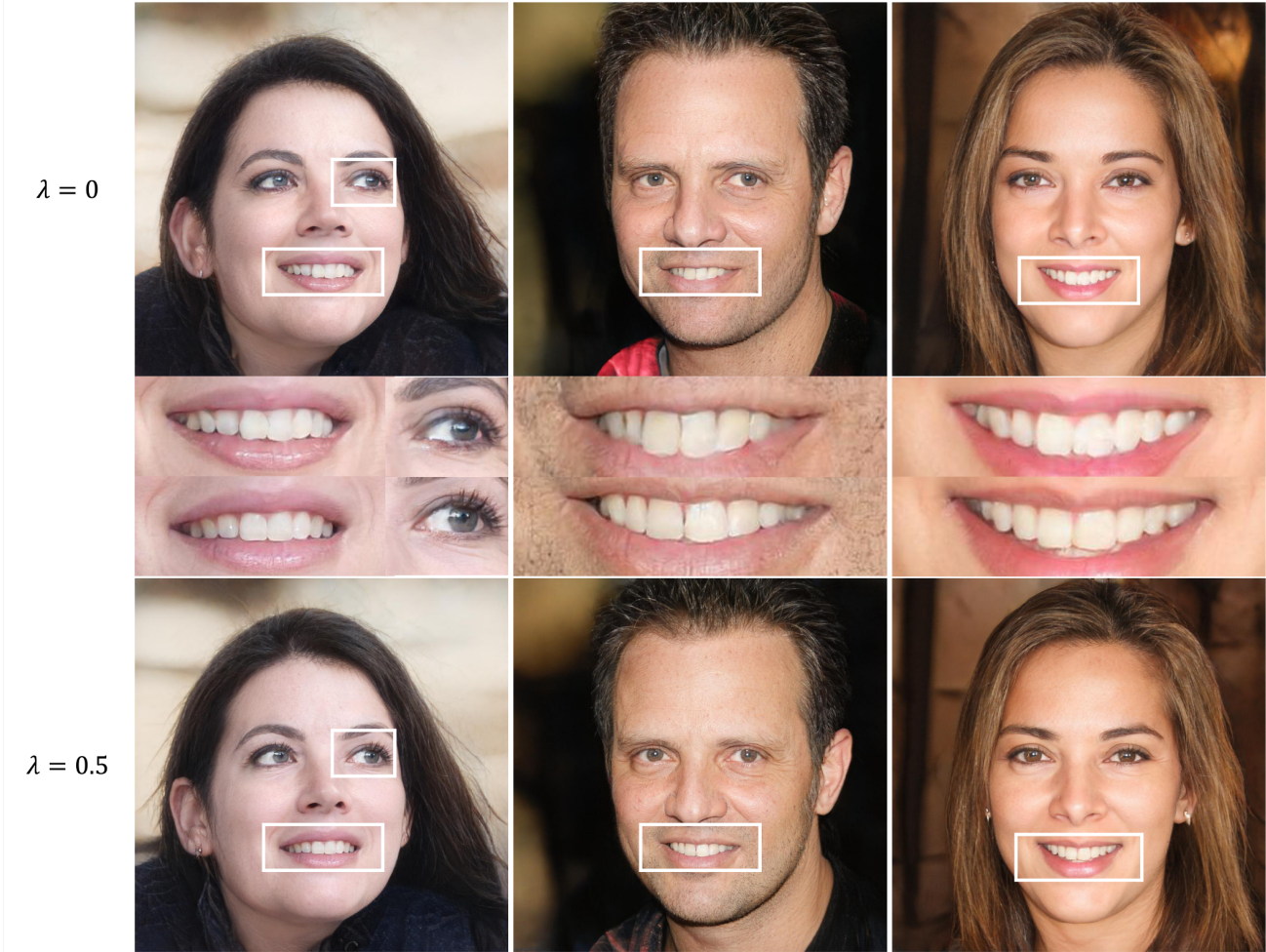


Figure 8: **Ablation study of image perception.** We show the inversion result from LSAP_E and the same encoder without \mathcal{L}_{NSCD} to illustrate the effect. LSAP_E significantly improves the image quality and solves the unnatural generation.

are shown in Table 4. A higher value of λ makes image distortion increase. This result is in line with our expectations since λ controls the contributions of alignment loss. Conversely, perception and editability are improved as λ increased. We visualize the inversion results in Figure 8 with $\lambda = 0$ and 0.5. In the first row, quality of teeth, eyes and

lip’s texture is weak. For example, in the left image in first row, the end of the left eyelid (right in the figure) is located too far from the left eye. Besides, teeth is misaligned with adhesions and lips are too smooth without normal texture. These problems are solved by LSAP, as we can see in the second row. To demonstrate change in editability, we fur-

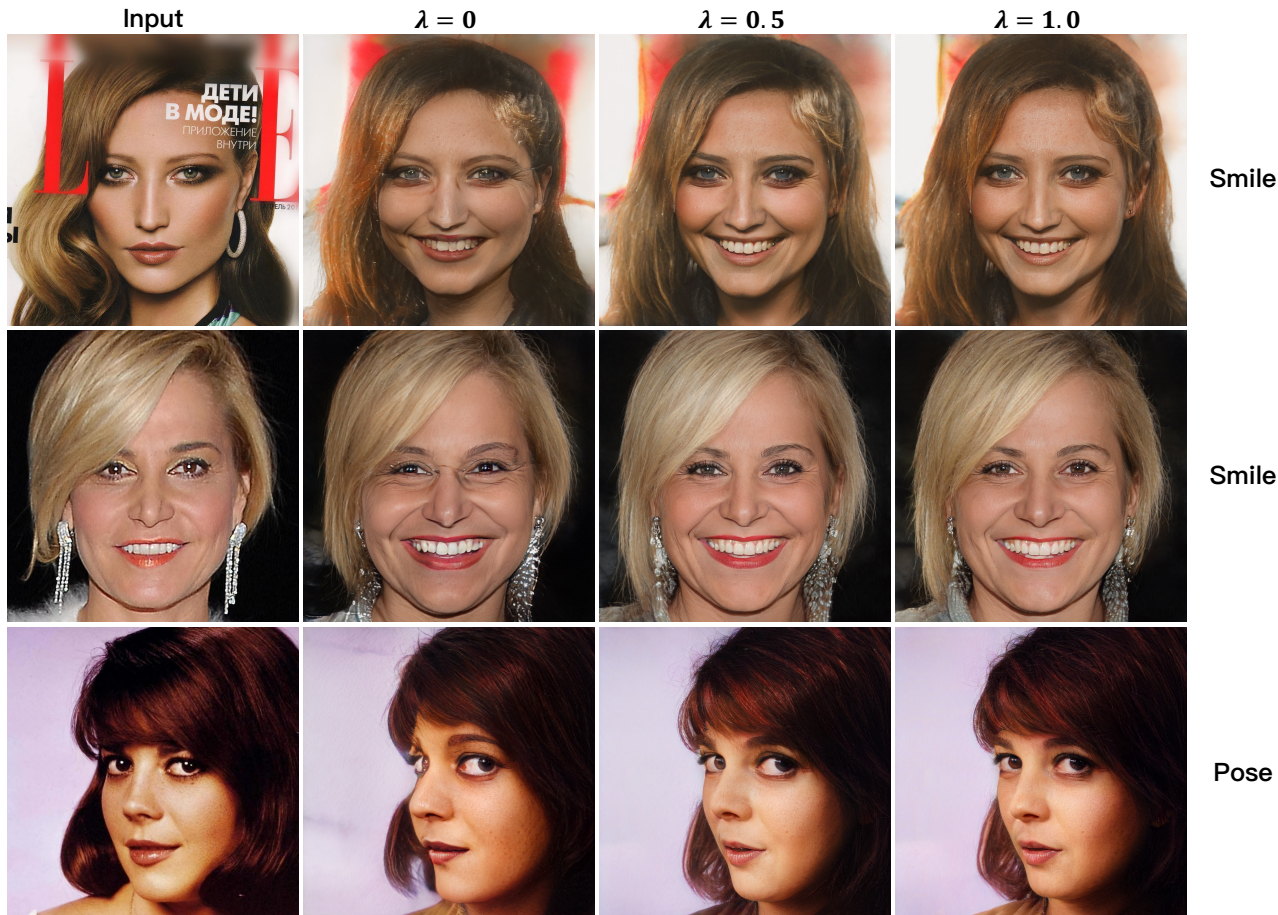


Figure 9: **Ablation study of image editability.** We show the manipulation result from LSAP_E with different hyper-parameter λ .

ther compare the manipulation results with $\lambda = 0, 0.5, 1.0$, which is shown in Figure 9. The first two images are edited with "smile" while the third is edited with "pose". When $\lambda = 0$, the edited images are unphotorealistic, and glasses occur with editing "smile". Results of $\lambda = 0.5$ and 1.0 show the similar results with excellent editability. The inversion and editing results show the superiority of our alignment paradigm.

D. Image Perception

We illustrate the discrepancy of image perception from each inversion method by high-resolution inverse images. As can be seen in Figure 10, the inverse results from each approach are marginally different in high resolution, especially in hair, teeth, lip, and skin area. This is not obvious in low resolution or thumbnails, as can be seen the first row. However, it makes image unnatural and fake in high resolution. We recommend comparing the visual quality at a higher resolution (e.g., 1024×1024). Our alignment

paradigm improves the image quality well, as can be seen in Figure 10, our results have natural visual details.

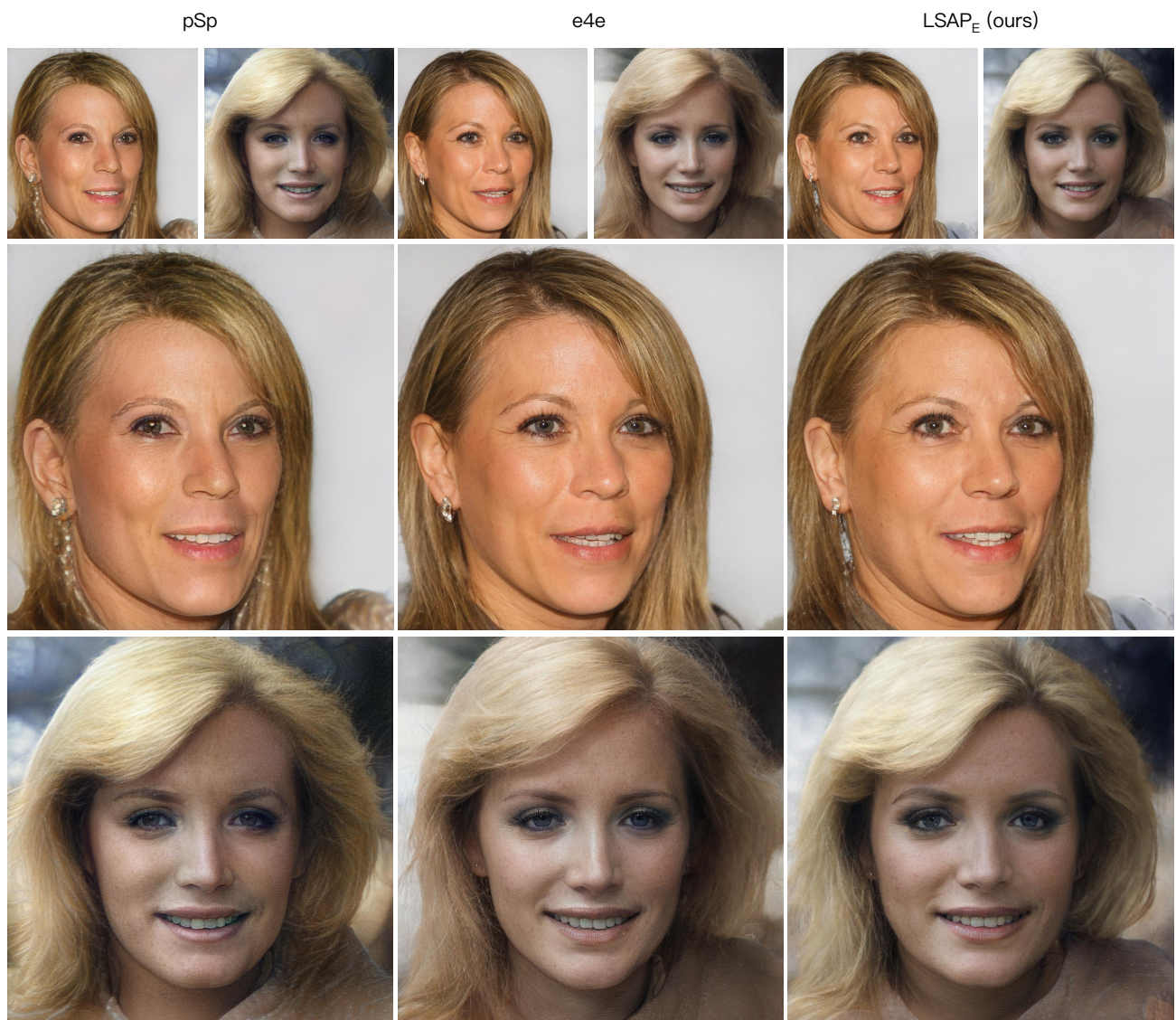


Figure 10: **Illustrate image perception in high resolution results.** We show the inversion results from pSp, e4e, and LSAP_E in high resolution to demonstrate the details of images. We also provide the low-resolution results to compare in the first row. The difference of perception is not obvious in low-resolution images.